Available online at www.sciencedirect.com

ScienceDirect

journal homepage: www.elsevier.com/locate/he

On the relative efficacy of electropermeation and isothermal desorption approaches for measuring hydrogen diffusivity

Alfredo Zafra [a], *Zachary Harris* [b], *Evzen Korec* [a], *Emilio Martínez-Pañeda* [a,*]

[a] *Department of Civil and Environmental Engineering, Imperial College London, London SW7 2AZ, UK*
[b] *Department of Mechanical Engineering and Materials Science, University of Pittsburgh, Pittsburgh, PA 15261, USA*

HIGHLIGHTS

- Permeation and desorption methods are used to measure hydrogen diffusivity in pure Fe.
- The first statistically significant comparison of isothermal desorption and permeation is provided.
- Isothermal desorption experiments reduce the coefficient of variation by 3-fold.
- Permeation is shown to be very sensitive to the electrochemical boundary conditions.
- Isothermal desorption provides accurate and repeatable diffusivity measurements.

GRAPHICAL ABSTRACT

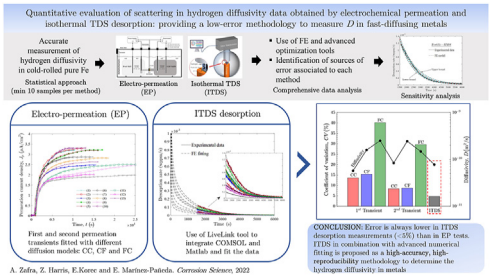

ARTICLE INFO

Article history:
Received 26 August 2022
Received in revised form
24 September 2022
Accepted 3 October 2022
Available online 25 October 2022

Keywords:
Hydrogen diffusion
Electro-permeation
TDS

ABSTRACT

The relative efficacy of electrochemical permeation (EP) and isothermal desorption spectroscopy (ITDS) methods for determining the hydrogen diffusivity is investigated using cold-rolled pure iron. The diffusivities determined from 13 first transient and 8 second transient EP experiments, evaluated using the conventional lag and breakthrough time methods, are compared to the results of 10 ITDS experiments. Results demonstrate that the average diffusivity is similar between the second EP transient and ITDS, which are distinctly increased relative to the first EP transient. However, the coefficient of variation for the ITDS experiments is reduced by 2 and 3-fold relative to the first and second EP transients, confirming the improved repeatability of ITDS diffusivity measurements. The source of the increased error in EP measurements is systematically evaluated, revealing an important influence of assumed electrochemical boundary conditions on the analysis and interpretation of EP experiments.

* *Corresponding author.*
E-mail address: e.martinez-paneda@imperial.ac.uk (E. Martínez-Pañeda).
https://doi.org/10.1016/j.ijhydene.2022.10.025

Isothermal desorption
Repeatability

Introduction

The deployment and safe operation of hydrogen transport and storage infrastructure is being threatened by the degradation of metals when exposed to hydrogen [1–3]. However, despite over a century of study [4–7], hydrogen-assisted cracking (HAC) remains a relevant failure mode for metallic structural components exposed to hydrogen-producing/containing environments across a number of industrial sectors [8]. Current best practices for designing against and prognosis of HAC involve the use of linear elastic fracture mechanics (LEFM)-based damage tolerant design [9–11]. While fundamentally robust, the implementation of LEFM-based approaches can be complicated by the sensitivity of HAC behavior to changes in microstructural [12–15], mechanical [16–18], and environmental [19–21] parameters. As such, it is critical that the influence of these factors be well understood when evaluating new alloy systems for use in hydrogen-rich environments.

From an environmental perspective, the parameters most pertinent to HAC are the diffusible hydrogen concentration ($C_{H,Diff}$) and the hydrogen diffusivity (D) in the material of interest [22–25]. Regarding the former, $C_{H,Diff}$ represents the hydrogen content available to participate in the hydrogen-assisted fracture process and is strongly dependent on the operative environment conditions (*i.e.*, solution composition/pH, electrochemical potential, hydrogen pressure/fugacity, etc. [5,19,26–30]). It is well-established that susceptibility to HAC is dependent on $C_{H,Diff}$. For example, the threshold stress intensity associated with the onset of hydrogen-assisted cracking (K_{TH}) has been observed to decrease as $C_{H,Diff}$ increases [31–34]; this dependence is explicitly incorporated into proposed models for K_{TH} [35–37]. Similarly, the Stage II hydrogen-assisted crack growth rate has been correlated with hydrogen diffusivity across a range of relevant alloy systems [38–40], particularly under severe hydrogen-producing conditions [18]. As with K_{TH}, the hydrogen diffusivity is a critical parameter in existing models for the Stage II crack growth rate [21,36].

These direct linkages between hydrogen-metal interaction parameters and HAC metrics underscores the importance of characterizing these factors when assessing the compatibility of a new alloy for use in aggressive environments [41,42]. While all hydrogen-metal interactions are critical to understand and contribute to HAC susceptibility, the hydrogen diffusivity is of particular importance given that it (1) affects the rate at which a given concentration is obtained in the material, and (2) is explicitly required for the interpretation of some hydrogen-metal interaction experiments (e.g., barnacle cell electrode [43]). There are two primary experimental methods for determining the hydrogen diffusivity [42]: permeation and thermal desorption. Permeation experiments are performed using a thin membrane of the material of interest that separates two environments. Hydrogen is generated on one side of the membrane, diffuses through the material, and exits the membrane at the other side, where the rate of hydrogen egress is measured [42]. For electrochemical permeation (EP) experiments, hydrogen uptake is driven by cathodically polarizing one side of the membrane and then measuring the current induced by hydrogen oxidation on the egress side [44]. Standard analysis methods are then used to determine the hydrogen diffusivity from the permeation data [45]. While permeation generally involves starting with nominally hydrogen-free specimens, diffusivity measurements using thermal desorption methods utilize samples that have ideally been hydrogen pre-charged with a spatially uniform hydrogen concentration. Samples are then placed into an ultra-high vacuum system, which is heated to a specific temperature (*i.e.*, isothermal conditions) and the rate of hydrogen egress is monitored with a mass spectrometer [46,47]. The diffusivity is then determined through fitting the hydrogen egress rate versus time profile using either numerical [48] or analytical methods [47].

While both approaches have been widely utilized in the open literature, each approach has been historically leveraged for a specific subset of conditions. Isothermal desorption spectroscopy (ITDS) is commonly employed for slow-diffusing materials and often involves large specimens to minimize the effects of hydrogen egress while the sample analysis chamber is brought to ultra-high vacuum and the selected isothermal condition is reached [46,47,49–51]. Conversely, EP is generally employed on thin (<1 mm thick) membranes of fast-diffusing material [44,52]. While data obtained from each method are often compared via literature sources, direct assessments of the relative efficacy of the two techniques are minimal given their use under distinct conditions. However, recent advances in thermal desorption systems, such as the introduction of conduction-based heating and improved vacuum system design for more rapid sample introduction, now enable the use of ITDS for material/sample combinations that were previously considered incompatible with this technique. For example, Zafra et al. [53] recently demonstrated that ITDS and EP methods yielded similar average diffusivities for thin (<1 mm thick) sheet specimens of cold-rolled pure Fe. Critically, this direct comparison revealed that the error in replicate ITDS measurements was noticeably reduced relative to the replicate EP experiments [53]. It is well-known that EP experiments are prone to significant scatter, which has been historically attributed to numerous factors: the need for sample conditioning prior to starting the permeation experiment [28,54–58], surface effects [59,60], trapping effects [61–63], concentration-dependent diffusion [64,65], analysis method assumptions [52,66–68], failure to reach true steady-state conditions [69], and test-to-test variations in specimen thickness, environmental parameters, among other [70,71]. The work of Zafra et al. [53] suggests that this longstanding issue of error in EP experiments may be circumvented via the more widespread adoption of ITDS, but this prior study only

performed two experiments per technique. As such, additional experiments are needed to more rigorously compare the ITDS and EP methods for measuring hydrogen diffusivity.

The objective of this study is to provide the first statistically significant comparison of EP and ITDS approaches for measuring hydrogen diffusivity. A total of 21 permeation experiments are performed on cold-worked pure iron and then analyzed using the standard breakthrough and lag time methods [45]. The EP experiments are then compared to the results of ten ambient temperature ITDS experiments. These large datasets are subsequently leveraged to comment on the relative accuracy of each technique, the importance of assumed boundary conditions when analyzing EP data, and the broader implications of these findings for the hydrogen community. The results obtained reveal a higher sensitivity of ITDS measurements and demonstrate its applicability to fast diffusion materials.

Experimental methods

Material

This study was conducted using cold-rolled pure iron procured in the as-rolled condition from Goodfellow Ltd. as a 1-mm thick sheet. The supplier reported a purity of >99.5 wt %Fe and a 50% reduction as the average degree of cold work. Permeation and TDS experiments were performed on plate specimens with nominal dimensions of 250 mm × 250 mm x 1 mm and 10 mm × 10 mm x 1 mm, respectively. The specimens were excised from the sheet using an abrasive saw. In order to ensure consistent surface conditions between experiments, both faces of every sample were mechanically ground using SiC papers, finishing with 1200 grit.

Hydrogen permeation tests

Thirteen EP experiments were performed at room temperature (22 ± 1 °C) using a modified Devanathan-Stachurski double-cell. The specimen thickness, L, was 0.92 ± 0.02 mm and a circular area of 2 cm^2 (16-mm diameter) was exposed to both sides of the double-cell.

The hydrogen reduction cell was filled with 3 wt. % NaCl solution and contained a typical three-cell electrode system, with a Pt counter electrode, silver/silver chloride (Ag/AgCl) reference electrode, and the sample as the working electrode. Hydrogen production was achieved by applying a cathodic current density, J_c, of 5 mA/cm^2 to the cold-rolled Fe membrane using a Gamry 1010B potentiostat operated in galvanostatic mode. The corresponding cathodic potential (vs. Ag/AgCl) was measured at the beginning of the test to ensure consistent charging conditions between specimens. The hydrogen oxidation cell was filled with 0.1 M NaOH solution and also contained a Pt counter electrode and Ag/AgCl reference electrode, with a second Gamry 1010B potentiostat operated in chronoamperometry mode to record the permeation current density, J_p, as a function of time. Both solutions were actively deaerated via bubbling with pure nitrogen, which was initiated 1 h before the beginning of the permeation test and continued through the end of the experiment. For each experiment, a thin Pd layer was electroplated onto the specimen surface facing the oxidation side of the double-cell to enhance the hydrogen oxidation reaction kinetics and avoid disturbances in the permeation signal from iron oxidation [72–74].

To ensure the efficient oxidation of hydrogen atoms reaching the anodic side of the specimen, the anodic surface was polarized at -25 ± 11 $mV_{Ag/AgCl}$, which corresponds to the nominal open-circuit potential (OCP) for this environment. The permeation current density was then allowed to stabilize until reaching a baseline below 0.1–0.2 μA/cm^2, after which the galvanostatic cathodic charging was started on the reduction side of the double-cell. A hydrogen concentration gradient is thus generated in the specimen, with hydrogen atoms permeating through the iron membrane from the cathodic to the anodic side. During the test, J_p describes an exponential rising transient until reaching a maximum permeation current density, which is commonly known as the steady-state permeation current, J_{ss}. Further details regarding the EP procedure as well as a schematic representation of the experimental setup (including the reduction and oxidation reactions) are provided elsewhere [53]. After completing the first permeation transient ($J_c = 5$ mA/cm^2), a second transient was performed on eight of the samples by increasing J_c to 10 mA/cm^2. These experiments were performed to assess whether the variability in diffusion coefficient would improve under conditions where surface and trapping effects on permeation are reduced [75].

Consistent with precedent literature [26,52,75–82] and current permeation testing standards [45,83], the hydrogen diffusion coefficient, D, of both permeation transients was determined using the breakthrough time and lag time methods, which are based on the following relationship:

$$D = \frac{L^2}{Mt} \tag{1}$$

where t and M are determined by which method is being employed. For the breakthrough method, M has a value of 6 and t is defined as the breakthrough time, t_{bt}, which corresponds to the time where $J_p/J_{ss} = 0.1$. Conversely, for the lag time method, M is equal to 15.3 and t is defined as the lag time, t_{lag}, which is determined by the time when $J_p/J_{ss} = 0.63$. Both approaches represent closed-form solutions of Fick's second law under the assumption that the hydrogen subsurface concentration is a constant, finite value at the entry side and zero at the exit side of the membrane.

Isothermal TDS tests (ITDS)

Ten ITDS experiments were performed on 0.90 ± 0.02 mm thick specimens using a thermal desorption spectroscopy (TDS) system. Each specimen was first pre-charged with hydrogen in deaerated 3 wt. % NaCl solution using a Gamry 1010B potentiostat operated in galvanostatic mode to maintain a constant cathodic current density of 5 mA/cm^2. The specimens were charged for 3 h to obtain a nominally uniform hydrogen concentration across the plate thickness, based on the previously reported hydrogen diffusivity for the current material heat [53]. ITDS measurements were performed under ultra-high vacuum (10^{-9} mbar) conditions using a previously

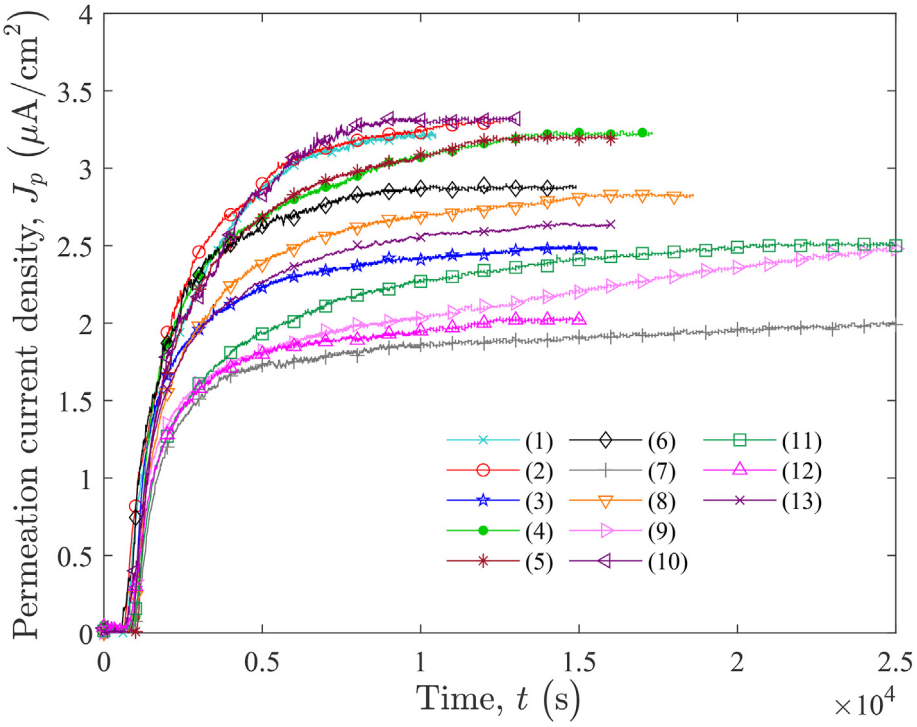

Fig. 1 – 1st permeation transients (J_c = 5 mA/cm^2) for cold-rolled pure Fe at 22 °C.

described TDS system [53] equipped with a regularly calibrated Hiden Analytical RC PIC quadrupole mass spectrometer with a hydrogen detection resolution of 4.4×10^{-6} wppm/s. The elapsed time between the completion of cathodic charging and the beginning of the ITDS experiment was 25 min. This is the minimum time needed to clean and dry the sample, load it into the system, and reach ultra-high vacuum conditions. All ITDS experiments were conducted at ambient temperature, which varied slightly across the test matrix (22.5 ± 0.5 °C), though the measured variation in temperature during a given individual experiment was always below ±0.1 °C. The rate of hydrogen egress (wppm/s) from the sample was then measured as a function of time for 6000 s.

The hydrogen diffusion coefficient, D_{iso}, was determined by fitting a 1-D finite element (FE) simulation of hydrogen transport to the measured ITDS profile (wppm/s vs. time) for each experiment. Recall that diffusion is governed by Fick's second law, which in a one-dimensional form reads:

$$\frac{\partial C}{\partial t} = D\frac{\partial^2 C}{\partial x^2} \tag{2}$$

where C is the diffusible hydrogen concentration. For the current study, it is assumed that a homogeneous hydrogen concentration exists across the specimen thickness at the start of the simulation (*i.e.*, $C = C_{0iso}$ at $t = 0$) and that the hydrogen concentration at the free surface is zero given the use of an ultra-high vacuum environment (*i.e.*, $C = 0$ at $x = \pm L/2$). A FE mesh sensitivity study demonstrated that mesh-independent results were efficiently obtained for a progressive mesh composed of 200 elements decreasing in size towards the free surface of the specimen. As all experiments were performed at ambient temperature (22 °C) and did not use the heater stage of the TDS, D_{iso} was determined in a single step analysis through fitting the experimentally-measured hydrogen desorption rate versus time data by iteratively changing the C_{0iso} and D_{iso} values. FE calculations were performed using the commercial package COMSOL Multiphysics and the LiveLink tool was employed to integrate COMSOL with Matlab, where a routine for parameter optimization was developed using the curve fit function `lsqcurvefit`, which performs a least square minimization using the Levenberg-Marquardt algorithm.[1]

Results

Permeation tests

The 1st permeation transients obtained for thirteen EP experiments performed on cold-rolled pure Fe at 22 °C are shown in Fig. 1. Each experiment was stopped once the permeation current density reached steady state, J_{ss1}, which was defined as a variation in permeation current density of less than 0.05 μA/cm^2 over a 1000 s interval. The specimen thickness (L), steady state permeation current density (J_{ss1}), breakthrough time (t_{bt}), lag time (t_{lag}), and hydrogen diffusivities obtained by means of the breakthrough (D_{bt1}) and time lag (D_{lag1}) methods are shown for each transient in Table 1. The mean and standard deviation for each of these parameters are also provided in the table.

Despite the clear differences in the measured permeation transients, Table 1 demonstrates that the average hydrogen diffusivity obtained by the breakthrough and lag time

[1] The COMSOL model and the Matlab fitting subroutine are made freely available at www.empaneda.com/codes.

Table 1 – 1st permeation transient parameters for cold-rolled pure Fe at 22 °C.

Test	L (mm)	J_{ss1} (μA/cm^2)	t_{bt1}(s)	D_{bt1} (m^2/s)	t_{lag1}(s)	D_{lag1} (m^2/s)
(1)	0.93	3.21	834	6.78×10^{-11}	2596	5.55×10^{-11}
(2)	0.90	3.30	776	6.76×10^{-11}	2224	6.01×10^{-11}
(3)	0.92	2.48	988	5.55×10^{-11}	1795	7.79×10^{-11}
(4)	0.93	3.22	1093	5.16×10^{-11}	2310	6.23×10^{-11}
(5)	0.92	3.20	1143	4.83×10^{-11}	2504	5.62×10^{-11}
(6)	0.88	2.87	753	6.69×10^{-11}	1845	6.97×10^{-11}
(7)	0.92	2.01	1087	5.13×10^{-11}	2158	6.59×10^{-11}
(8)	0.91	2.83	1025	5.33×10^{-11}	2458	5.67×10^{-11}
(9)	0.90	2.49	953	5.58×10^{-11}	2808	4.83×10^{-11}
(10)	0.93	3.31	945	5.99×10^{-11}	2635	5.48×10^{-11}
(11)	0.92	2.51	1088	5.04×10^{-11}	2886	4.85×10^{-11}
(12)	0.94	2.02	928	6.16×10^{-11}	1998	7.30×10^{-11}
(13)	0.91	2.63	1007	5.40×10^{-11}	2203	6.29×10^{-11}
Average	0.92	2.78	971	5.72×10^{-11}	2340	6.09×10^{-11}
SD	0.02	0.46	123	0.68×10^{-11}	346	0.90×10^{-11}

methods are very similar (5.72 and 6.09 $\times$ 10^{-11} m^2/s, respectively). This observation differs from a prior study conducted on this same material heat [53], which reported a >30% difference in the hydrogen diffusivity from the breakthrough and lag time approaches. However, it should be noted that this previous effort only performed two EP measurements and the present data demonstrates that an appreciable range of calculated diffusivities are possible for a given method (e.g. 4.83 to 7.79 $\times$ 10^{-11} m^2/s for the lag time approach). Such results strongly suggest that large EP test matrices are necessary to obtain reliable hydrogen-metal interaction metrics.

After the completion of the 1st permeation transient, a 2nd permeation transient was performed on eight of the experiments by increasing J_c to 10 mA/cm^2. As both hydrogen trapping [84] and unsteady surface conditions [85] will be attenuated during the 2nd transient, it is expected that the scatter in the calculated hydrogen diffusivity should be reduced relative to the 1st transient. The curves corresponding to the 2nd transient are shown in Fig. 2, which demonstrates that each experiment reached a stable permeation current density (J_{ss2}), within 10,000 s. J_{ss2}, along with t_{bt2}, t_{lag2} and the associated hydrogen diffusivities (D_{bt2} and D_{lag2}) are reported in Table 2. The mean and standard deviation for each of these parameters are also included in the table. As noted for the 1st permeation transient, the average hydrogen diffusivities obtained for the 2nd transient using the breakthrough and lag time methods are very similar, 8.64 and 8.22 $\times$ 10^{-11} m^2/s respectively. However, these values are approximately 1.5 times higher than the diffusivities that were calculate from the 1st permeation transient (5.72–6.09 $\times$ 10^{-11} m^2/s), consistent with a reduced contribution of hydrogen trapping [79, 82, 84, 86].

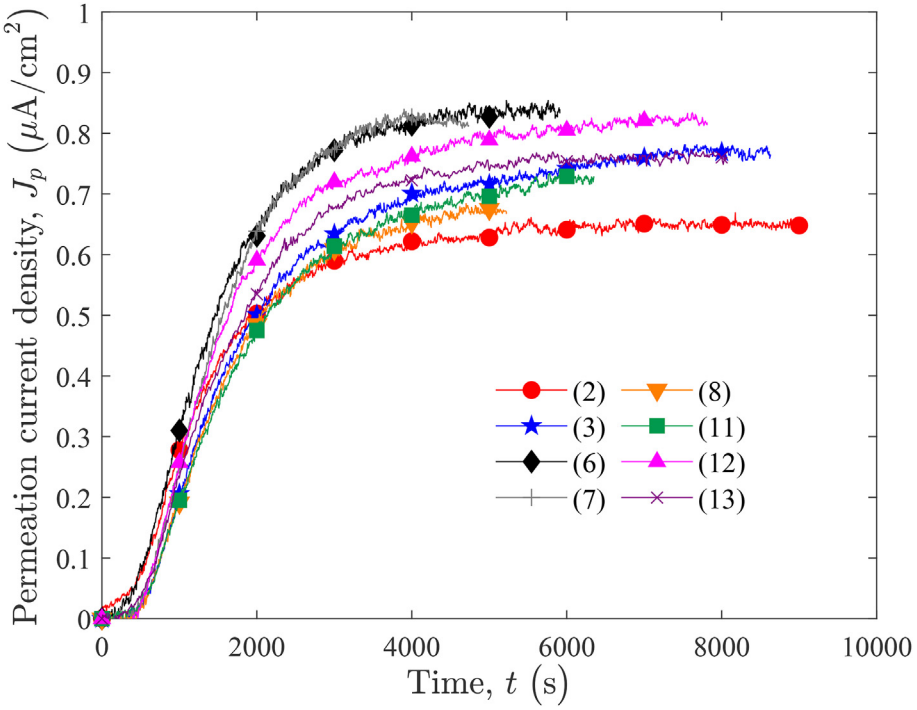

Fig. 2 – 2nd permeation transients (J_c = 10 mA/cm^2) for cold-rolled pure Fe at 22 °C.

Table 2 – 2nd permeation transient parameters for cold-rolled pure Fe at 22 °C.

Test	L (mm)	J_{ss2} (μA/cm^2)	t_{bt2}(s)	D_{bt2} (m^2/s)	t_{lag2}(s)	D_{lag2} (m^2/s)
(2)	0.90	0.65	525	9.99×10^{-11}	1473	9.08×10^{-11}
(3)	0.92	0.77	702	7.81×10^{-11}	1892	7.39×10^{-11}
(6)	0.88	0.84	518	9.73×10^{-11}	1514	8.49×10^{-11}
(7)	0.92	0.82	687	8.12×10^{-11}	1660	8.57×10^{-11}
(8)	0.91	0.67	680	8.03×10^{-11}	1715	8.12×10^{-11}
(11)	0.92	0.72	682	8.05×10^{-11}	1880	7.44×10^{-11}
(12)	0.94	0.82	640	8.93×10^{-11}	1681	8.67×10^{-11}
(13)	0.91	0.76	640	8.49×10^{-11}	1730	8.01×10^{-11}
Average	0.91	0.76	634	8.64×10^{-11}	1693	8.22×10^{-11}
SD	0.02	0.07	73	0.83×10^{-11}	150	0.60×10^{-11}

Isothermal TDS tests

The hydrogen desorption rate versus time profiles measured during ten ITDS experiments conducted at 22 °C are shown in Fig. 3. The best fit to Fick's second law, determined from finite element (FE) simulations, is indicated by the corresponding dashed lines. For all cases, the FE calculations closely capture the experimental behavior. The initial diffusible hydrogen concentration (C_{0iso}) and diffusion coefficient (D_{iso}) that yielded the best fit of the experimental curve, as well as the coefficient of determination, R^2, which provides a goodness-of-fit measure, are reported in Table 3. C_{0iso} represents the area below the ITDS profile starting from $t = 0$. The mean and standard deviation for these two parameters are provided at the bottom of the table. Two observations can be made from these data. First, the standard deviation for D_{iso}

Table 3 – Initial diffusible hydrogen concentration, C_{0iso}, and diffusivity values, D_{iso}, determined from ITDS experiments.

Test	L (mm)	C_{0iso} (wppm)	D_{iso} (m^2/s)	R^2
(1)	0.87	0.43	7.27×10^{-11}	0.988
(2)	0.90	0.27	7.98×10^{-11}	0.992
(3)	0.92	0.40	8.20×10^{-11}	0.985
(4)	0.90	0.63	8.02×10^{-11}	0.991
(5)	0.90	0.71	7.72×10^{-11}	0.994
(6)	0.88	0.84	8.00×10^{-11}	0.985
(7)	0.86	0.50	7.94×10^{-11}	0.989
(8)	0.92	0.17	7.28×10^{-11}	0.990
(9)	0.93	0.21	7.23×10^{-11}	0.993
(10)	0.91	0.48	7.97×10^{-11}	0.986
Average	0.90	0.46	7.76×10^{-11}	0.989
SD	0.02	0.22	0.36×10^{-11}	0.003

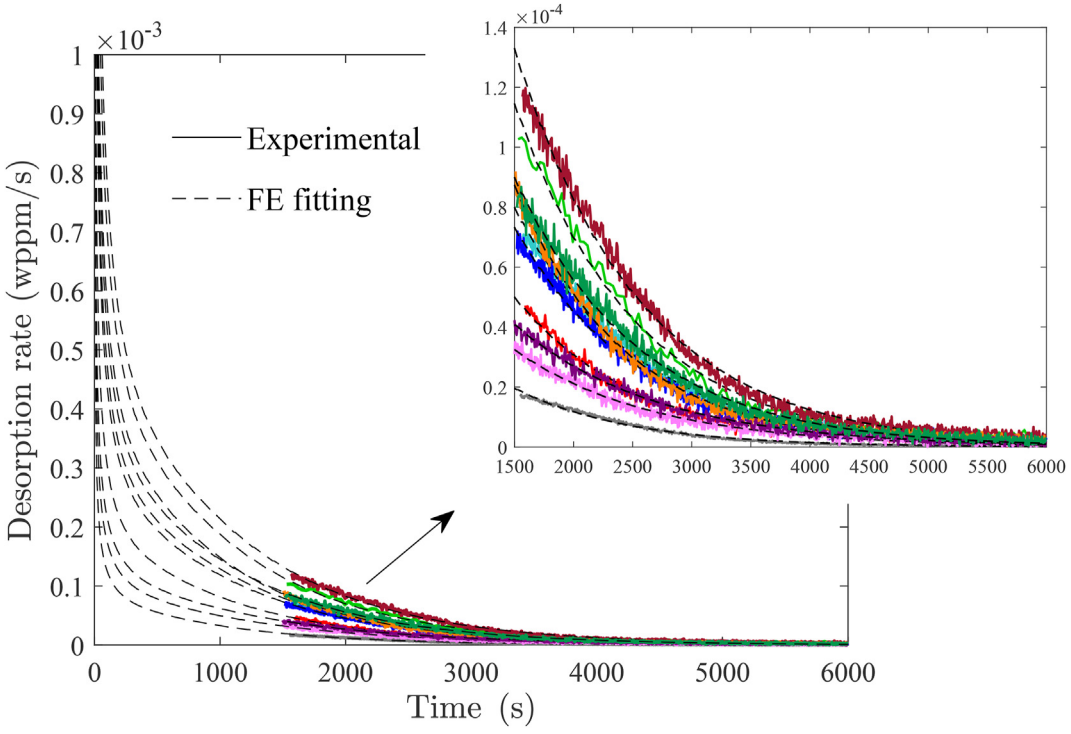

Fig. 3 – Experimental hydrogen desorption rate vs. time profiles obtained from ITDS experiments performed at 22 °C (solid lines) and the best fit determined from finite element analysis (dashed lines).

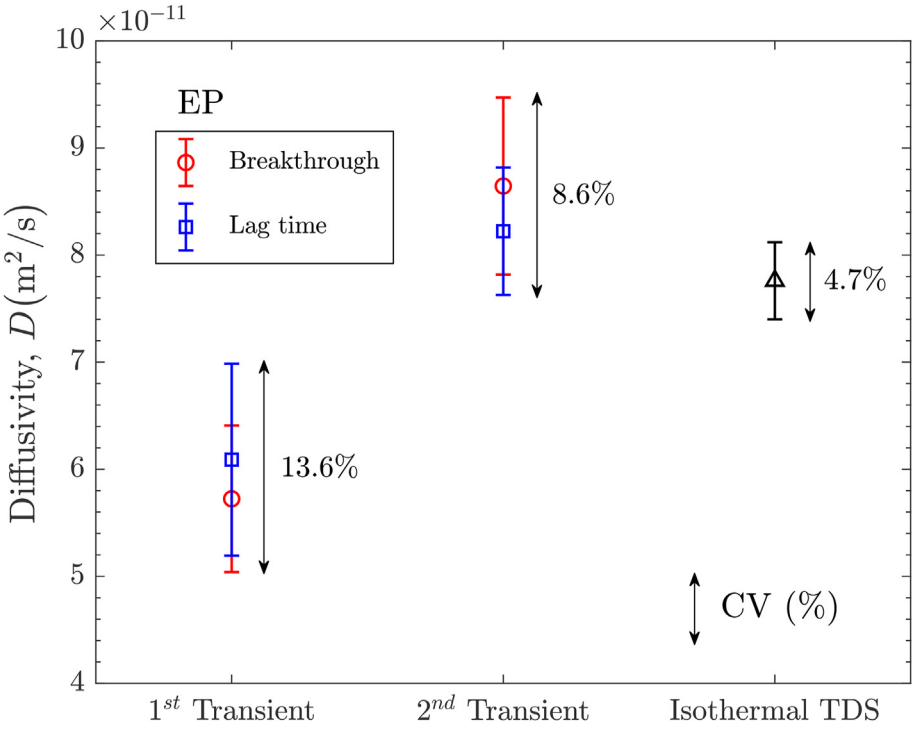

Fig. 4 – Average diffusivity and standard deviation (represented by the error bars) obtained from electropermeation (1st and 2nd transients) and ITDS experiments. The coefficient of variation CV(%), indicated by the black arrows, is also included for each group.

(0.36×10^{-11} m^2/s) is generally half of the standard deviation observed across the permeation approaches. Second, the average D_{iso} lies in between the diffusivities observed for the first and second permeation transients, but notably closer to the second transient result.

Discussion

The preceding results provide a comprehensive dataset that can be leveraged to compare the relative efficacy of EP and ITDS methods for determining hydrogen diffusivity. The objectives of the following discussion are: (1) comment on the diffusivities calculated amongst the tested approaches, (2) identify the factors likely responsible for the test-to-test scatter that exists in each technique, and (3) discuss the implications of these results in the context of the optimal approach for assessing hydrogen diffusivity.

Comparison of diffusivities obtained in EP and ITDS experiments

Fig. 4 shows the average diffusivity and standard deviation (represented by the error bars) obtained from the 1st and 2nd transients of the permeation experiments (breakthrough and lag time methods) as well as the ITDS experiments. The coefficient of variation (CV), which is defined as the ratio of the standard deviation and the mean, is also provided to quantify the dispersion in the measured hydrogen diffusivity for each approach, and is represented by black arrows in Fig. 4.

Three observations are notable from the summary presented in Fig. 4. First, for a given permeation transient, the lag time and breakthrough time methods yield nominally identical results, with the average of one approach always well within the error bars of the other. Second, ITDS yields a similar average hydrogen diffusivity as the 2nd permeation transient (~7.8 vs. ~8.4 $\times$ 10^{-11} m^2/s), with both being increased relative to the diffusivity measured during the 1st permeation transient (~6 $\times$ 10^{-11} m^2/s). Lastly, both the standard deviation and CV are significantly reduced for the ITDS experiments as compared to the permeation experiments, with the CV being nearly half and one-third of that observed for the 2nd and 1st permeation transients, respectively.

Considering the first observation, recall that the lag time and breakthrough time approaches represent closed-form solutions to Fick's second law for the same boundary conditions. In other words, these methods represent two points along the same normalized flux (J_p/J_{ss}) versus time curve. As long as the assumed boundary conditions for these solutions are generally reasonable for the performed experiment, it follows that the two approaches should yield similar average diffusivity values. Regarding the second observation, the improved agreement in the average hydrogen diffusivities measured using the 2nd permeation transient and ITDS methods relative to the 1st transient is consistent with expectations for the boundary conditions of each experiments. Specifically, while the 1st permeation transient begins with a nominally hydrogen-free membrane, the 2nd permeation transient and ITDS experiments both start with a nominally uniform, non-zero hydrogen content across the specimen thickness. As such, trapping effects should be attenuated

during the 2nd permeation transient and ITDS experiments, resulting in an increased hydrogen diffusivity relative to the 1st transient.

Lastly, the most striking observation from the present data in Fig. 4 is the reduced scatter in the ITDS-measured diffusivity as compared to the permeation-based measurements. While prior work reported a lower error for ITDS-based measurements [53], this previous study only performed a small number of experiments. The current work confirms the increased precision of ITDS relative to EP for a much larger experimental matrix (⩾ 10 of each kind). Critically, the present results also highlight the propensity for increased error in EP experiments relative to ITDS, regardless of employed analysis approach or the use of multiple transients. Interestingly, the difference in the CV between the 1st (13.6%) and 2nd (8.6%) transients suggests that only a fraction of error in EP experiments is likely related to trapping influences, suggesting that other factors provide a more significant contribution to the error in EP experiments.

Identification of the sources of error

Sources of error in EP tests

Several authors have previously outlined the factors that may affect the repeatability of EP measurements [59,70,71,87]. These prior efforts have collectively established that hydrogen uptake and transport in metals during EP tests is sensitive to the following broad categories:

(i) Solution composition/pH and temperature. These factors can influence the amount of absorbed hydrogen as well as trap occupancy, which will modify the hydrogen diffusivity. While variations in these parameters would induce scattering in EP experiments, they are not considered a likely source of error in the current experiments due to the significant efforts made to control these variables.

(ii) Trapping phenomena. The rate of transport of hydrogen atoms through the membrane is affected by both reversible and irreversible trapping [84,88]. Variability in this effect could manifest in two ways: (1) sample-to-sample variations in trap site characteristics and (2) evolution in the efficacy of trapping as the permeation experiment progresses and traps are filled. While the former cannot be rigorously excluded, all samples were prepared from the same plate of Fe using the same approaches to minimize such effects. An effect of the latter is clearly demonstrated by the results in Fig. 4, where the diffusivity during the 2nd transient was notably increased relative to that measured in the 1st transient. However, the fact that the 2nd transient still exhibits elevated levels of scatter suggests that trapping is not the primary source of the observed variations in EP data.

(iii) Surface effects. The specimen's surface condition and thickness play an essential role in minimizing surface effects during hydrogen permeation through a metal membrane. Typically, a well-polished surface [89], the application of surface catalysts such as palladium coatings [90,91] or the use of hydrogen recombination poisons [92,93] are employed to minimize surface effects on hydrogen dissociation and subsequent uptake into the membrane. Additionally, it is important that the sample be sufficiently thick such that these surface effects do not dominate over bulk diffusivity. Prior work demonstrated that surface effects in pure Fe are minimal for samples with thicknesses larger than 0.5 mm [29]. While this suggests that surface effects are not the likely source of scatter in the current experiments, the influence of subtle differences in Pd layer thickness on the oxidation side of the cell and surface finish on the reduction side cannot be completely neglected. A possible role of surface effects on the scatter would also be consistent with postulated sources of error for permeation measurements in the literature [52,61,70].

(iv) Boundary conditions at the entry and the exit surfaces. The use of galvanostatic or potentiostatic charging can modify the boundary conditions on the reduction side of the EP experiment and therefore determine the most appropriate method of analysis of the permeation transient [67,91,94]. Assuming incorrect boundary conditions can have a significant impact on the average diffusivity [67], while scatter can also be induced by failing to fully meet the assumed boundary conditions (*i.e.*, due to a passive film) or through the evolution of the boundary conditions during an EP experiment.

While trapping influences cannot be completely ruled out, the above review indicates that assumed boundary conditions (and the role of surface effects on those boundary conditions) likely provides a more significant contribution to the increased error observed in the EP measurements. In the following section, the importance and influence of assumed boundary conditions on the calculated hydrogen diffusivity is assessed through the application of three models for EP.

Influence of assumed boundary conditions for analysis of permeation data

In the majority of the literature, the hydrogen diffusivity is determined from EP data using the breakthrough and lag time methods [95]. These approaches are employed due to their closed-form nature, which avoids the need for more complex fitting algorithms. However, it is important to note that these methods represent specific solutions (at $J_p/J_{ss} = 0.1$ and 0.63, respectively) to Fick's second law for 1-D permeation under the boundary conditions of a constant hydrogen concentration of some finite amount at the membrane's entry side ($C_{x=0} = C_{0app}$) and of zero at the exit side ($C_{x=L} = 0$). Under such constant concentration (CC) conditions, the complete normalized permeation flux as a function of time relationship is described by:

$$\frac{J_p}{J_{ss}} = 1 + 2\sum_{n=1}^{\infty}(-1)^n \exp\left(-\frac{n^2\pi^2 D_{CC} t}{L^2}\right) \quad (3)$$

where L is the specimen thickness and D_{CC} is the diffusivity for these assumed boundary conditions. Critically, this model (and therefore the lag time and breakthrough time solutions) is only rigorously applicable to EP experiments conducted using potentiostatic conditions on the reduction side of the permeation cell [67,91]. This arises from the fact that the

hydrogen fugacity, and therefore concentration, is directly related to the hydrogen overpotential, which is established by the applied electrochemical potential and solution composition [44]. This requirement can be functionally met using galvanostatic charging so long as the surface conditions and environment do not change [71]. Such a scenario results in a nominally constant applied potential on the specimen surface, but careful monitoring is required to confirm compliance with this boundary condition.

While it is possible to apply the CC model to EP experiments conducted under galvanostatic charging conditions, it is most rigorous to evaluate such experiments with a constant flux (CF) model. This model assumes 1-D permeation under a constant hydrogen flux at the entry side of the membrane ($J_{x=0} = -FJ_c$) and a hydrogen concentration of zero at the exit surface ($C_{x=L} = 0$) [91,94]:

$$\frac{J_p}{J_{ss}} = 1 - \frac{4}{\pi}\sum_{n=0}^{\infty}\frac{(-1)^n}{2n+1}\exp\left(-\frac{(2n+1)^2\pi^2 D_{CF}t}{4L^2}\right) \quad (4)$$

While the CC and CF models represent idealized conditions that do not consider surface effects [67], hydrogen uptake in a real system will depend on the kinetics of the following absorption-desorption reaction:

$$H_{adsorbed} \underset{K_{des}}{\overset{K_{abs}}{\rightleftharpoons}} H_{absorbed} \quad (5)$$

Several authors have attempted to account for these surface effects through the development of more complex permeation models [67,91,94,96]. For example, the flux continuity (FC) model was first proposed by Wang [96] to describe hydrogen gas permeation while taking into account absorption and desorption reactions. Zhang et al. [91] simplified the absorption-desorption reactions used in the FC model and applied several assumptions (e.g., similar surface conditions at the entry and exit surfaces, and constant surface coverage (θ) with permeation time), which allowed the extension of this model to describe EP experiments. The normalized permeation flux as a function of time for these assumptions is then expressed as:

$$\frac{J_p}{J_{ss}} = 1 + 2(2+\xi)\sum_{n=1}^{\infty}\frac{\xi\cos(\eta_n) - \eta_n\sin(\eta_n)}{\eta_n^2 + \xi^2 + 2\xi}\exp\left(-\frac{(\eta_n)^2 D_{FC}t}{L^2}\right) \quad (6)$$

where ξ is the ratio between the desorption constant k_{des} and the diffusion constant D/L in the metal, and the dimensionless parameter η_n is the nth positive root of:

$$tan(\eta_n) = \frac{2\xi\eta_n}{\eta_n^2 - \xi^2} \quad (7)$$

As the desorption constant, k_{des}, is analogous to a surface-limited mass transfer coefficient [90], a lower k_{des} implies an increased effect of the surface on the overall mass transport. Therefore, the ξ parameter can be used as a proxy for the relative influence of surface effects on the permeation transient, where a reduction in ξ similarly indicates an increased role of hydrogen absorption and desorption during permeation. In addition to explicitly incorporating surface influences, the FC model provides a more general solution to the permeation problem, which under specific conditions result in the FC modeling becoming identical to either the CC or CF models. For example, if the value of ξ becomes sufficiently large or small, then the FC model reduces to the CC and CF models, respectively [67,91]. However, this generality comes at the cost of increased analysis complexity relative to the CC and CF models since both the diffusivity, D_{FC}, and ξ must be numerically determined.

To assess the effect of assumed boundary conditions, every permeation transient was iteratively fit to each model using Matlab with the diffusivity being the free parameter for the CC and CF model, while both the diffusivity and ξ parameter were fit for the FC model. As shown in Fig. 5 for two representative 1st and 2nd transients, all three models reasonably describe each permeation transient as quantified by the R^2 coefficients listed in the figure, though subtle differences can be identified. For example, the CF and FC models yield the best (and nominally identical) fits to the first permeation transients (Fig. 5a and b); the good agreement of the CF model is consistent with expectations given the use of galvanostatic charging in the current experiments. Conversely, the 2nd permeation transients (Fig. 5c and d) are best fit by the CC model (which is identical for this case to the FC model). While the 2nd transient was also conducted under galvanostatic conditions, these results indicate that the surface was sufficiently conditioned to enable a CC-like boundary condition [71].

The diffusivities D_{CC}, D_{CF}, D_{FC}, and ξ determined for each 1st and 2nd transient measurement, along with the R^2 for each fitting are provided in Supplementary material. The mean and standard deviation for these parameters are listed in Table 4, while a barplot of the CV for each model's calculated diffusivity is shown in Fig. 6. These fitted parameters reveal two key observations. First, the calculated hydrogen diffusivity is strongly dependent on the applied model, with nearly five-fold and four-fold difference observed for the 1st and 2nd transients, respectively. Critically, these differences exist despite the models exhibiting similar goodness of fit to the experimental data (e.g., the CF and FC model during the 1st transient and the CC and FC model during the 2nd transient). Second, the choice of boundary conditions also has an influence on the observed scatter of permeation experiments. For example, the FC model has an approximately 3-fold larger CV (reaching 40% for the 1st transient) relative to the CC and CF models, which had generally similar CV values. Such increased variability for the FC model is likely driven by the need to fit two independent parameters (D_{FC} and ξ). Lastly, it is interesting to note that the lowest error observed across the full fit approaches is 8%. Zhang et al. [86] reported a similar error (~11%) for a large (~5 specimen) EP test matrix that was analyzed with full-fitting methods, while Svoboda and co-workers [79] observed an 8% error when analyzing a large number of duplicate EP experimental pairs via full-fitting. Such data suggests that an error of 8–10% may be the lower-bound error for the EP method.

The preceding analysis underscores the difficulty of rigorously interpreting EP data, since the applicability of a given model is affected by the employed electrochemical boundary conditions (which may evolve during an experiment) and whether or not to consider absorption/desorption kinetics. While uncertainties associated with choosing the best model to fit experimental data always exist, EP fitting appears unique in that similarly well-fit models (e.g., the CC and FC model fits

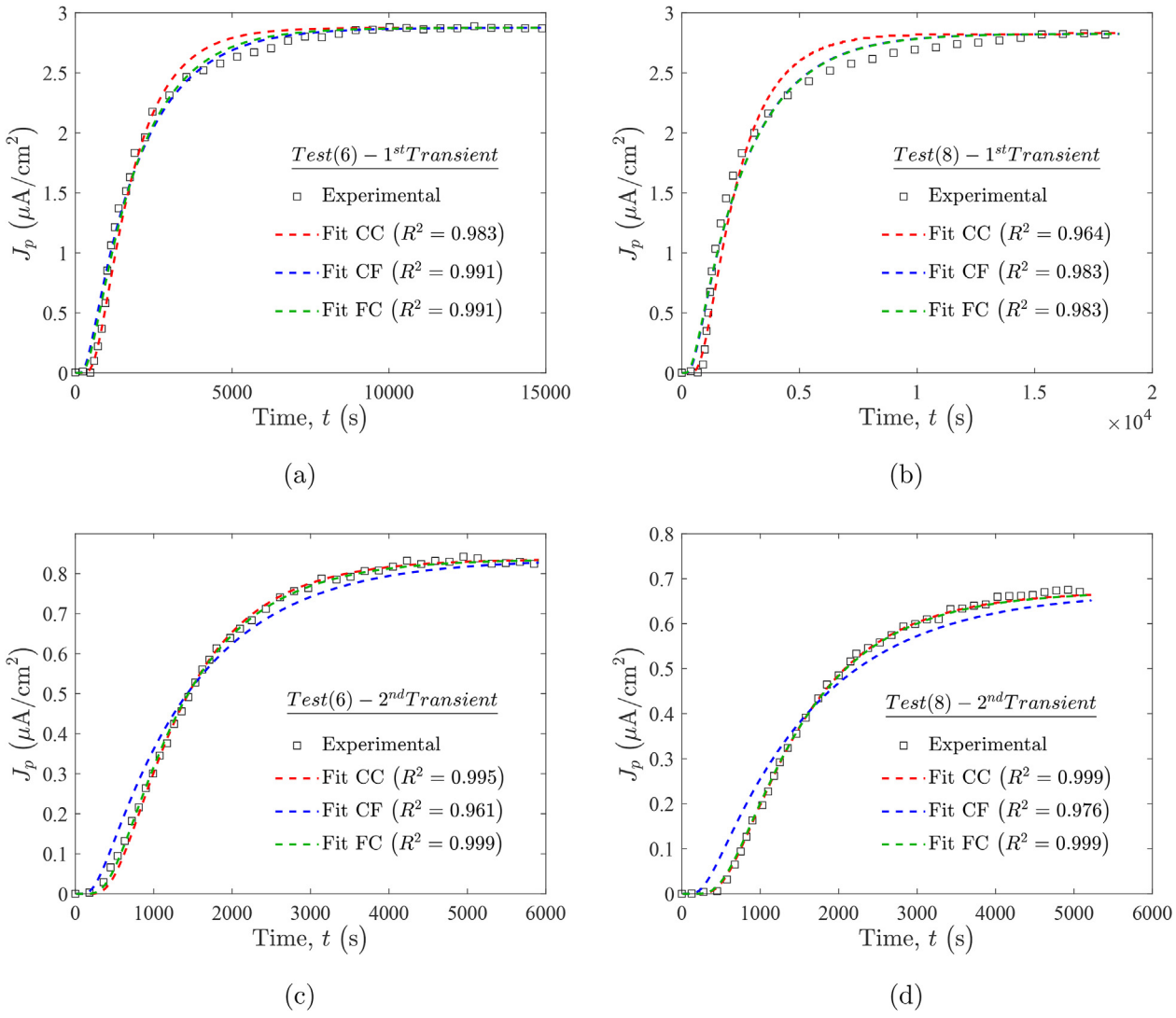

Fig. 5 – Comparison of the CC, CF, and FC model fits to two representative (a, b) 1st and (b, c) 2nd transient EP experiments.

Table 4 – Diffusivity values obtained in the 1st and 2nd transients of all the permeation experiments by fitting the CC, CF and FC models.

Transient	Value	Constant Concentration		Constant Flux		Flux Continuity		
		D_{CC} (m^2/s)	R^2	D_{CF} (m^2/s)	R^2	D_{FC} (m^2/s)	ξ	R^2
1st	Average	5.76×10^{-11}	0.938	1.60×10^{-10}	0.963	2.53×10^{-10}	1.09	0.965
	SD	0.79×10^{-11}	0.09	0.25×10^{-10}	0.06	1.03×10^{-10}	0.49	0.04
2nd	Average	8.42×10^{-11}	0.996	2.44×10^{-10}	0.985	1.49×10^{-10}	7.0	0.998
	SD	0.71×10^{-11}	0.003	0.21×10^{-10}	0.01	0.44×10^{-10}	4.8	0.002

to the 2nd EP transient) yield two-to-three fold differences in best-fit diffusivity. In other words, the choice of model itself for interpreting EP data becomes a source of error for EP experiments. This observation is consistent with the conclusions of other authors [67, 68, 91], who have each suggested that the primary challenge for EP methods is ensuring the theoretical conditions assumed EP data analysis are valid for the employed experimental conditions. Critically, these challenges are magnified by the widespread use of simple closed-form solutions (e.g., the lag and breakthrough time methods). Such approaches are convenient, but do not provide feedback on the overall goodness of the chosen model's fit and can lead to potential misinterpretations. For example, variations between lag time and breakthrough time calculations often are attributed to trapping effects, which undoubtedly affect EP measurements [88], especially during 1st transients. However, such differences could be simply driven by the inherent scatter in EP experiments (the results of the 2nd permeation transient CC model, where trapping and surface effects appear to be minimized, suggests a minimum CV of 8%) or

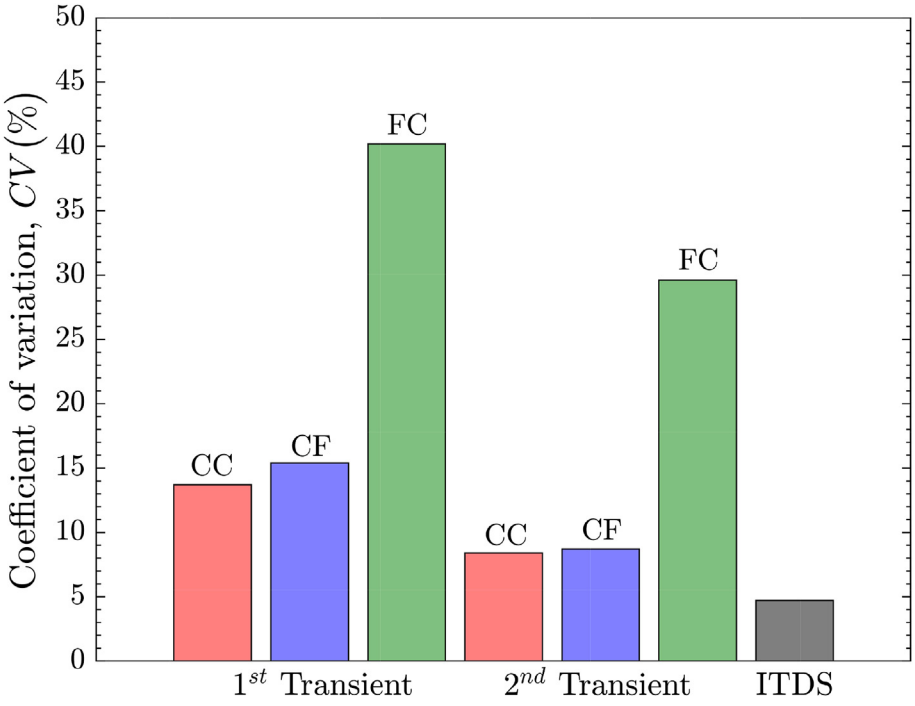

Fig. 6 – Coefficient of variation, CV, associated to each method.

poor agreement with the actual boundary conditions of the experiment (Fig. 6). While leveraging a full fit approach will not solve all these challenges, it will provide insights into whether the use of the CC model-based simple lag time and breakthrough time approaches is justified.

Sources of error in ITDS experiments

As shown in Fig. 6, hydrogen diffusivity measurements conducted using ITDS have considerably less error than measurements using EP methods. This reduction in error is likely attributed to three factors. First, ITDS uses hydrogen egress from a pre-charged sample to establish the material diffusivity; therefore, the equilibrium hydrogen trap distribution will be reached during the precharging step. This reduces trapping effects during the subsequent desorption experiment and explains the reasonable agreement between the average diffusivities measured with ITDS and the 2nd permeation transient. Second, the reduced error in ITDS experiments also manifests from the analysis approach. Specifically, the hydrogen diffusivity is calculated from the gradient in the desorbed hydrogen concentration rate (wppm/s) with time rather than the magnitude of the hydrogen concentration vs time (as happens in EP experiments, where the permeation current is proportional to the hydrogen concentration [68,97–99]). As such, subtle deviations in diffusivity induce noticeable changes in the ITDS fit, resulting in a concomitant increase in sensitivity for this approach.

To highlight the sensitivity of the ITDS analysis, a representative ITDS desorption curve (Run 5) and the associated COMSOL-Matlab best fit (red dashed line) are plotted in Fig. 7. The best fit diffusivity (7.72×10^{-11} m^2/s) for this experiment was then modified by the CV (8.5%) from the 2nd EP transient (CC model) to establish upper (8.36×10^{-11} m^2/s) and lower (7.07×10^{-11} m^2/s) bound diffusivities. The hydrogen desorption curves for these modified diffusivities were then calculated, keeping C_{0iso} from the original fit (0.71 wppm), to assess how the best-case EP error would affect the ITDS fit results. These upper and lower fits are shown by the black dashed lines in Fig. 7, which clearly depart from the experimental ITDS data, demonstrating that even an 8% change in the diffusivity will distinctly affect the goodness of the ITDS fit.

Lastly, the boundary conditions associated with ITDS are well-defined and the majority of the important variables are readily controlled or explicitly known (e.g., specimen thickness, time between the end of charging and the start of the ITDS measurement). In fact, the primary source of scatter in ITDS variable is likely the initial hydrogen concentration (C_{0iso}) introduced during the pre-charging. As reported in Ref. [53], the measured hydrogen concentration at the end of precharging can vary appreciably, even when significant efforts are made to keep all charging parameters identical. As such, it is important to evaluate whether or not the C_{0iso} value calculated from the ITDS experiment fits is a realistic value. One pathway to assess the reasonableness of C_{0iso} is to compare it to the calculated surface hydrogen concentration (C_{0app}) on the entry side of the EP experiment. Since both the ITDS and 1st transients used galvanostatic charging at 5 mA/cm^2, these two approaches should yield similar values. Regarding C_{0app}, it can be calculated as follows:

$$C_{0app} = \frac{J_{ss1}L}{DF} \tag{8}$$

where L is the membrane thickness, D the diffusion coefficient, J_{ss1} is the steady state permeation current, and F is Faraday's constant; note that Eq. (8) assumes the CC model boundary conditions. According to Table 3, C_{0iso} is 0.46 ± 0.22 wppm, while the C_{0app} calculated from Table 1 using the CC method results is 0.59 ± 0.13 wppm. While the average EP-

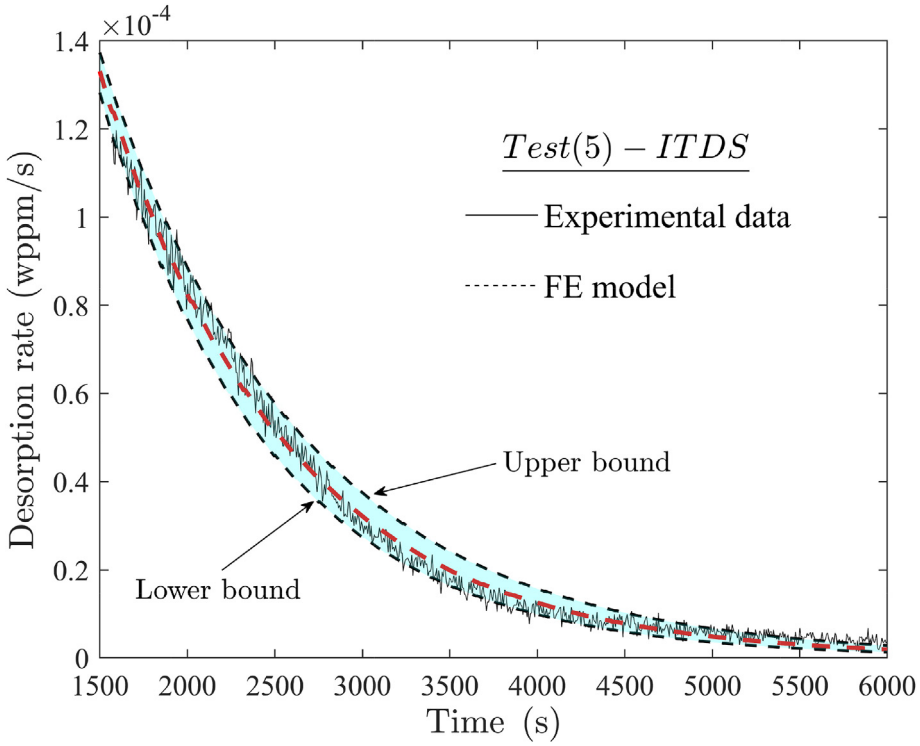

Fig. 7 – Fitted ITDS curve with lower and upper bounds determined with the lowest coefficient of variation (8.4%) associated to the second permeation transient (CC model).

calculated surface concentration is slightly higher than that calculated for the ITDS, significant overlap in error bars exists between the two approaches, suggesting that the fitted C_{0iso} and therefore the ITDS fitting methodology are reasonable.

Implications of results

The preceding results and discussion provide an opportunity to comment on the general efficacy of the ITDS and EP approaches for determining hydrogen diffusivity. First, the present data confirm the utility of the ITDS approach for assessing hydrogen diffusivity relative to EP methods, consistent with prior work by the authors [53]. Despite using a fast diffusing material (cold-rolled pure Fe) in a thin sheet geometry (<1 mm thick), which has historically been incompatible with ITDS [47], the ITDS and EP (especially the 2nd transient) experiments yielded similar average hydrogen diffusivities. Additionally, good agreement was observed between the averages of the calculated surface hydrogen concentration in the EP experiments (C_{0app}) and the calculated initial hydrogen concentration for the ITDS experiments (C_{0iso}). However, while these average metrics were often in reasonable agreement, the scatter in diffusivity from the EP experiments was always at least 2 times higher than that observed in ITDS experiments (Figs. 4 and 6), irrespective of analysis strategy and permeation transient.

Second, the current results suggest that the increased scatter in EP experiments is likely driven by variations in electrochemical boundary conditions due to surface conditions, with a secondary contribution from hydrogen trapping. Comparison of three different diffusion models for EP revealed a substantial influence (up to five-fold differences) of these boundary conditions on both the average diffusivity (Table 4) and scatter (Fig. 6). Such results have several practical implications. For example, it is common in the literature to analyze EP data, even results generated with galvanostatic charging, using the conventional lag and breakthrough time methods. However, these analysis strategies are closed form solutions to the CC model, while galvanostatic charging provides a boundary condition more in line with the CF model. This can result in misleading evaluations since the fits for the CC and CF models to EP data can be reasonably similar (Fig. 5), but the CF model consistently yields a three-fold higher diffusivity than the CC model. Additionally, if galvanostatic boundary conditions are employed, it should be recognized that the applied electrochemical potential will likely vary from specimen to specimen as well as throughout the experiment due to surface influences, particularly during a 1st transient experiment. These influences will eventually be attenuated [71], but inherently introduce error into the analysis that will especially influence short permeation experiments (such as the case for fast-diffusing materials like pure Fe). Based on these observations, it is suggested that EP experiments be conducted using potentiostatic approaches. This suggestion is driven by: (1) the fact that the standard lag time and breakthrough time solutions are derived from the CC model, which is best aligned with a potentiostatic experiment, (2) the established relationship between applied electrochemical potential and hydrogen fugacity [44], which sets the surface hydrogen concentration, and (3) a reduction in surface effect variations since the evolution of the applied potential that occurs during galvanostatic charging can be avoided.

Lastly, while ITDS appears to be ideal for determining the hydrogen diffusivity, there are limitations to this approach that should be noted. For example, ITDS may be less effective than EP for materials with strong passive films (Al, Ti, etc.) that could hinder hydrogen desorption until sufficiently high temperatures are reached that reduce the oxide. In this instance, electrochemical techniques may be advantageous due to the strong control of all the variables, *i.e.*, they allow one to apply the current density necessary to reduce these oxides. Additionally, ITDS requires the use of specialized ultra-high vacuum capabilities that can be quite expensive. As such, it should be underscored that EP remains an important and useful tool for assessing hydrogen-metal interactions, but it requires special care and attention to detail to ensure that artifacts are not unknowingly introduced.

Conclusions

A comparison of the hydrogen diffusivity obtained via EP and ITDS methods has been performed leveraging the results of $\geq$10 replicate experiments for each approach conducted on cold-rolled pure Fe. Based on these results, the following conclusions can be made:

- The average diffusivity obtained from a 1st permeation transient using the standard breakthrough and lag time methods was distinctly lower (~5.8×10^{-11} cm^2/s) than that observed using these same methods on a consecutively run 2nd permeation transient (~8.4×10^{-11} cm^2/s). The observed variation across the replicate permeation experiments decreased from 13.6% to 8.6% between the 1st and 2nd permeation transient, respectively. Interestingly, the average diffusivity measured from the ITDS experiments was nominally similar to the 2nd permeation transient (~7.8×10^{-11} cm^2/s), but the variation was reduced by nearly half.
- The efficacy of the ITDS analysis approach is supported by the close agreement between the best-fit initial hydrogen concentration for the ITDS specimen and the hydrogen concentration calculated for the entry surface of the permeation specimen.
- The increased scatter in the EP measurements relative to the ITDS experiments was attributed to both an influence of hydrogen trapping and the assumed electrochemical boundary conditions in common EP analysis approaches. The similarity in average diffusivity, but strong difference in scatter, between the ITDS and 2nd permeation transient results suggests that trapping likely provides a secondary contribution relative to electrochemical boundary condition effects.
- The influence of electrochemical boundary conditions on the hydrogen diffusivity calculated from EP experiments was assessed by fitting three different diffusion models to the large set of generated EP data, *i.e.*, constant concentration (CC) constant (CF) and flux continuity (FC). Not only was the average diffusivity sensitive to the applied boundary conditions (up to four-fold difference for the 2nd permeation transient), but the observed scatter also strongly depends on the employed model (CV ranged from 8% to 30% for the 2nd permeation transient).
- These data confirm the improved repeatability of ITDS for determining the hydrogen diffusivity in materials amenable to this technique. For materials where EP may be preferred (e.g., those with resilient passive films), the presented results underscore the need for closely controlling the electrochemical boundary conditions.

Potential avenues for future work include extending the demonstration of the ITDS approach to other materials, including oxide-bearing case studies.

Declaration of competing interest

The authors declare that they have no known competing financial interests or personal relationships that could have appeared to influence the work reported in this paper.

Acknowledgements

The authors acknowledge financial support from the EPSRC (grants EP/V04902X/1, EP/R010161/1 and EP/V009680/1). E. Martínez-Pañeda was additionally supported by an UKRI Future Leaders Fellowship [grant MR/V024124/1].

Appendix A. Supplementary data

Supplementary data to this article can be found online at https://doi.org/10.1016/j.ijhydene.2022.10.025.

REFERENCES

[1] Bouledroua O, Hafsi Z, Djukic MB, Elaoud S. The synergistic effects of hydrogen embrittlement and transient gas flow conditions on integrity assessment of a precracked steel pipeline. Int J Hydrogen Energy 2020;45(35):18010–20.
[2] Cerniauskas S, Jose Chavez Junco A, Grube T, Robinius M, Stolten D. Options of natural gas pipeline reassignment for hydrogen: cost assessment for a Germany case study. Int J Hydrogen Energy 2020;45(21):12095–107.
[3] Eames I, Austin M, Wojcik A. Injection of gaseous hydrogen into a natural gas pipeline. Int J Hydrogen Energy 2022;47(61):25745–54.
[4] Johnson WH. On some remarkable changes produced in iron and steel by the action of hydrogen and acids. Nature 1875;11(281):393.
[5] Gangloff RP, Somerday BP. Gaseous hydrogen embrittlement of materials in energy technologies. Cambridge: Woodhead Publishing Limited; 2012.
[6] Robertson IM, Sofronis P, Nagao A, Martin ML, Wang S, Gross DW, Nygren KE. Hydrogen embrittlement understood, metallurgical and materials transactions B: process metallurgy and materials. Process Sci 2015;46(3):1085–103.
[7] Djukic MB, Bakic GM, Sijacki Zeravcic V, Sedmak A, Rajicic B. The synergistic action and interplay of hydrogen embrittlement mechanisms in steels and iron: localized plasticity and decohesion. Eng Fract Mech 2019;216:106528.

[8] Gangloff RP. Hydrogen-assisted cracking. In: Milne I, Ritchie R, Karihaloo B, editors. Comprehensive structural integrity, vol. 6. New York, NY: Elsevier Science; 2003. p. 31–101.
[9] Gangloff RP. Probabilistic fracture mechanics simulation of stress corrosion cracking using accelerated laboratory testing and multi-scale modeling. Corrosion 2016;72(7):862–80.
[10] del Busto S, Betegón C, Martínez-Pañeda E. A cohesive zone framework for environmentally assisted fatigue. Eng Fract Mech 2017;185:210–26.
[11] Valverde-González A, Martínez-Pañeda E, Quintanas-Corominas A, Reinoso J, Paggi M. Computational modelling of hydrogen assisted fracture in polycrystalline materials. Int J Hydrogen Energy 2022;47(75):32235–51.
[12] Pallaspuro S, Yu H, Kisko A, Porter D, Zhang Z. Fracture toughness of hydrogen charged as-quenched ultra-high-strength steels at low temperatures. Mater Sci Eng 2017;688:190–201.
[13] Harris ZD, Burns JT. The effect of isothermal heat treatment on hydrogen environment-assisted cracking susceptibility in Monel K-500. Mater Sci Eng 2019;764(June):138249.
[14] Lin M, Yu H, Wang X, Wang R, Ding Y, Alvaro A, Olden V, He J, Zhang Z. A microstructure informed and mixed-mode cohesive zone approach to simulating hydrogen embrittlement. Int J Hydrogen Energy 2022;47(39):17479–93.
[15] Shoemaker TK, Harris ZD, Burns JT. Comparing stress corrosion cracking behavior of additively manufactured and wrought 17-4PH stainless steel. Corrosion 2022;78(6):528–46.
[16] Wang M, Akiyama E, Tsuzaki K. Crosshead speed dependence of the notch tensile strength of a high strength steel in the presence of hydrogen. Scripta Mater 2005;53(6):713–8.
[17] Álvarez G, Peral LB, Rodríguez C, García TE, Belzunce FJ. Hydrogen embrittlement of structural steels: effect of the displacement rate on the fracture toughness of high-pressure hydrogen pre-charged samples. Int J Hydrogen Energy 2019;44(29):15634–43.
[18] Harris ZD, Dubas EM, Popernack AS, Somerday BP, Burns JT. Elucidating the loading rate dependence of hydrogen environment-assisted cracking in a Ni-Cu superalloy. Theor Appl Fract Mech 2021;111:102846.
[19] McMahon ME, Harris ZD, Scully JR, Burns JT. The effect of electrode potential on stress corrosion cracking in highly sensitized Al–Mg alloys. Mater Sci Eng 2019;767:138399.
[20] Steiner PJ, Harris ZD, Vicente Moraes C, Kelly RG, Burns JT. Investigation of IG-SCC growth kinetics in Al-Mg alloys in thin film environments. Corrosion 2021;77(8):838–52.
[21] Gangloff RP, Ha HM, Burns JT, Scully JR. Measurement and modeling of hydrogen environment-assisted cracking in monel K-500. Metall Mater Trans A 2014;45(9):3814–34.
[22] San Marchi C, Somerday B. Technical reference for hydrogen compatibility of materials. Sandia Report; 2012.
[23] Oudriss A, Fleurentin A, Courlit G, Conforto E, Berziou C, Rébéré C, Cohendoz S, Sobrino JM, Creus J, Feaugas X. Consequence of the diffusive hydrogen contents on tensile properties of martensitic steel during the desorption at room temperature. Mater Sci Eng 2014;598:420–8.
[24] Zafra A, Peral LB, Belzunce J, Rodríguez C. Effect of hydrogen on the tensile properties of 42CrMo4 steel quenched and tempered at different temperatures. Int J Hydrogen Energy 2018;43(18):9068–82.
[25] Martínez-Pañeda E, del Busto S, Niordson CF, Betegón C. Strain gradient plasticity modeling of hydrogen diffusion to the crack tip. Int J Hydrogen Energy 2016;41(24):10265–74.
[26] Turnbull A, Saenz de Santa Maria M, Thomas ND. The effect of H2S concentration and pH on hydrogen permeation in AISI 410 stainless steel in 5% NaCl. Corrosion Sci 1989;29(1):89–104.
[27] Zakroczymski T, Szklarska-Śmiałowska Z, Smialowski M. Effect of arsenic on permeation of hydrogen through steel membranes polarized cathodically in aqueous solution. Mater Corros 1975;26(8):617–24.
[28] Liu Q, Atrens AD, Shi Z, Verbeken K, Atrens A. Determination of the hydrogen fugacity during electrolytic charging of steel. Corrosion Sci 2014;87:239–58.
[29] Kittel J, Feaugas X, Creus J. Impact of charging conditions and membrane thickness on hydrogen permeation through steel: thick/thin membrane concepts revisited. NACE - Int Corrosion Conf Ser 2016;2:858–78.
[30] Cupertino Malheiros L, Oudriss A, Cohendoz S, Bouhattate J, Thébault F, Piette M, Feaugas X. Local fracture criterion for quasi-cleavage hydrogen-assisted cracking of tempered martensitic steels. Mater Sci Eng 2022;847:143213.
[31] Lee Y, Gangloff RP. Measurement and modeling of hydrogen environment-assisted cracking of ultra-high-strength steel. Metall Mater Trans A 2007;38 A(13):2174–90.
[32] Li D, Gangloff RP, Scully JR. Hydrogen trap states in ultrahigh-strength AERMET 100 steel. Metall Mater Trans A 2004;35 A(3):849–64.
[33] Kehler BA, Scully JR. Predicting the effect of applied potential on crack tip hydrogen concentration in low-alloy martensitic steels. Corrosion 2008;64(5):465–77.
[34] Harris ZD, Dolph JD, Pioszak GL, Rincon Troconis BC, Scully JR, Burns JT. The effect of microstructural variation on the hydrogen environment-assisted cracking of monel K-500. Metall Mater Trans A 2016;47(7):3488–510.
[35] Akhurst KN, Baker TJ. Threshold stress intensity for hydrogen-induced crack growth. Metall Trans A 1981;12 A(6):1059–70.
[36] Gerberich WW. Modeling hydrogen induced damage mechanisms in metals. In: Gangloff RP, Somerday B, editors. Gaseous hydrogen embrittlement of materials in energy technologies, vol. II. Woodhead Publishing; 2012. p. 209–46.
[37] Martínez-Pañeda E, Niordson CF, Gangloff RP. Strain gradient plasticity-based modeling of hydrogen environment assisted cracking. Acta Mater 2016;117:321–32.
[38] Gangloff RP. Science-based prognosis to manage structural alloy performance in hydrogen. In: Somerday B, Sofronis P, Jones R, editors. Effects of hydrogen on materials: proceedings of the 2008 international hydrogen conference. Jackson Lake: ASM International; 2009. p. 1–21.
[39] Colombo C, Fumagalli G, Bolzoni F, Gobbi G, Vergani L. Fatigue behavior of hydrogen pre-charged low alloy Cr-Mo steel. Int J Fatig 2015;83:2–9.
[40] Shinko T, Halm D, Benoit G, Hénaff G. Controlling factors and mechanisms of fatigue crack growth influenced by high pressure of gaseous hydrogen in a commercially pure iron. Theor Appl Fract Mech 2021;112:102885.
[41] Gangloff RP. H-enhanced deformation and fracture in the crack tip process zone. In: Somerday BP, Sofronis P, editors. Materials performance in hydrogen environments: proceedings of the 2016 international hydrogen conference. Jackson Lake: ASME Press; 2016. p. 1–35.
[42] Depover T, Verbeken K. Hydrogen diffusion in metals: a topic requiring specific attention from the experimentalist. In: Van der Voorde M, editor. Hydrogen storage for sustainability, vol. II. Berlin: Walter de Gruyter GmbH; 2021. p. 247–80. Ch. 6.
[43] DeLuccia J, Berman D. An electrochemical technique to measure diffusible hydrogen in metals (barnacle electrode). In: Mansfeld F, Bertocci U, editors. Electrochemical corrosion testing, ASTM STP 727. American Society for Testing and Materials; 1981. p. 256–73.
[44] Subramanyan P. Electrochemical aspects of hydrogen in metals. In: Bockris J, Conway B, Yeager E, White R, editors. Comprehensive treatise on electrochemistry. New York: Plenum Press; 1981. p. 411–62.

[45] ISO 17081:2013 - method of measurement of hydrogen permeation and determination of hydrogen uptake and transport in metals by an electrochemical technique. International Organization for Standardization; 2014.
[46] Yamabe J, Sezgin J-G, Wada K. Interpretation of complex, tensile-fracture phenomena in precipitation-hardened, martensitic stainless steels, 17-4PH, in presence of hydrogen. Mater Sci Eng, A 2021;823:141717.
[47] Mine Y, Narazaki C, Murakami K, Matsuoka S, Murakami Y. Hydrogen transport in solution-treated and pre-strained austenitic stainless steels and its role in hydrogen-enhanced fatigue crack growth. Int J Hydrogen Energy 2009;34(2):1097–107.
[48] Díaz A, Cuesta II, Martínez-Pañeda E, Alegre JM. Influence of charging conditions on simulated temperature-programmed desorption for hydrogen in metals. Int J Hydrogen Energy 2020;45:23704–20.
[49] Yamabe J, Awane T, Matsuoka S. Investigation of hydrogen transport behavior of various low-alloy steels with high-pressure hydrogen gas. Int J Hydrogen Energy 2015;40(34):11075–86.
[50] Ai JH, Ha HM, Gangloff RP, Scully JR. Hydrogen diffusion and trapping in a precipitation-hardened nickel-copper-aluminum alloy Monel K-500 (UNS N05500). Acta Mater 2013;61(9):3186–99.
[51] Hurley C, Martin F, Marchetti L, Chêne J, Blanc C, Andrieu E. Numerical modeling of thermal desorption mass spectroscopy (TDS) for the study of hydrogen diffusion and trapping interactions in metals. Int J Hydrogen Energy 2015;40(8):3402–14.
[52] Boes N, Züchner H. Electrochemical methods for studying diffusion, permeation and solubility of hydrogen in metals. J Less Common Met 1976;49(C):223–40.
[53] Zafra A, Harris Z, Sun C, Martínez-Pañeda E. Comparison of hydrogen diffusivities measured by electrochemical permeation and temperature-programmed desorption in cold-rolled pure iron. J Nat Gas Sci Eng 2022;98:104365.
[54] Xie SX, Hirth JP. Permeation of hydrogen, trapping, and damage in spheroidized aisi 1090 steel. Corrosion 1982;38(9):486–93.
[55] Zakroczymski T. Effect of straining on the transport of hydrogen in iron, nickel, and stainless steel. Corrosion 1985;41(8):485–9.
[56] Chen JM, Wu JK. Hydrogen diffusion through copper-plated AISI 4140 steels. Corrosion Sci 1992;33(5):657–66.
[57] Bruzzoni P, Carranza RM, Collet Lacoste JR, Crespo EA. Hydrogen diffusion in α-iron studied using an electrochemical permeation transfer function. Electrochim Acta 1999;44(16):2693–704.
[58] Zhou P, Li W, Zhao H, Jin X. Role of microstructure on electrochemical hydrogen permeation properties in advanced high strength steels. Int J Hydrogen Energy 2018;43(24):10905–14.
[59] Kiuchi K, McLellan RB. The solubility and diffusivity of hydrogen in well-annealed and deformed iron. Acta Metall 1983;31(7):961–84.
[60] Addach H, Berçot P, Rezrazi M, Takadoum J. Study of the electrochemical permeation of hydrogen in iron. Corrosion Sci 2009;51(2):263–7.
[61] Kumnick AJ, Johnson HH. Hydrogen transport through annealed and deformed Armco iron. Metall Trans A 1974;5:1199–206.
[62] Lee JY, Lee JL. A trapping theory of hydrogen in pure iron. Philos Mag A: Phys Condens Matt Struct Defect Mech Prop 1987;56(3):293–309.
[63] Pundt A, Kirchheim R. Hydrogen in metals: microstructural aspects. Annu Rev Mater Res 2006;36(1):555–608.
[64] Ono K, Rosales L. On the anomalous behavior of hydrogen in iron at lower temperatures. Trans Metallurgical Soc AIME 1968;242:244–8.
[65] Zafra A, Belzunce FJ, Rodríguez C, Fernández-Pariente I. Hydrogen embrittlement of the coarse grain heat affected zone of a quenched and tempered 42CrMo4 steel. Int J Hydrogen Energy 2020;45(33):16890–908.
[66] Carvalho JP, Vilar EO, Araújo BA. A critical review and experimental analysis of the equation recommended by ASTM G148-97 and ISO 17081: 2004 for the calculation of the hydrogen diffusivity in metals and alloys. Int J Hydrogen Energy 2017;42(1):681–8.
[67] Montella C. Discussion on permeation transients in terms of insertion reaction mechanism and kinetics. J Electroanal Chem 1999;465(1):37–50.
[68] Pound B. Electrochemical techniques to study hydrogen ingress in metals. In: Bockris J, Conway B, White R, editors. Modern aspects of electrochemistry, vol. 25. New York: Plenum Press; 1993.
[69] Nelson H, Stein J. NASA TN D-7265: gas-phase hydrogen permeation through alpha iron, 4130 steel, and 304 stainless steel from less than 100°C to near 600°C. Moffat Field, CA: Tech. rep., Ames Research Center; 1973.
[70] Gonzalez O. The measurement of hydogen permeation in alpha iron: an analysis of experiments. Transactions of the Metallurgical Society of AIME 1969;245:607–12.
[71] Turnbull A. Factors affecting the reliability of hydrogen permeation measurement. Mater Sci Forum 1995;192–194:63–78.
[72] Devanathan MAV, Stachurski Z. The adsorption and diffusion of electrolytic hydrogen in palladium. Proc Roy Soc Lond Math Phys Sci 1962;270(1340):90–102.
[73] Driver R. Electrodeposition of Palladium on iron and steels for hydrogen permeation measurements. J Electrochem Soc 1981;128(11):1–3.
[74] Manolatos P, Jerome M, Galland J. Necessity of a palladium coating to ensure hydrogen oxidation during electrochemical permeation measurements on iron. Electrochim Acta 1995;(7):867–71.
[75] Zafra A, Belzunce J, Rodríguez C. Hydrogen diffusion and trapping in 42CrMo4 quenched and tempered steel: influence of quenching temperature and plastic deformation. Mater Chem Phys 2020:123599.
[76] Luppo MI, Ovejero-Garcia J. The influence of microstructure on the trapping and diffusion of hydrogen in a low carbon steel. Corrosion Sci 1991;32(10):1125–36.
[77] Wu JK. Electrochemical method for studying hydrogen in iron, nickel and palladium. Int J Hydrogen Energy 1992;17(12):917–21.
[78] Frappart S, Oudriss A, Feaugas X, Creus J, Bouhattate J, Thébault F, Delattre L, Marchebois H. Hydrogen trapping in martensitic steel investigated using electrochemical permeation and thermal desorption spectroscopy. Scripta Mater 2011;65(10):859–62.
[79] Svoboda J, Mori G, Prethaler A, Fischer FD. Determination of trapping parameters and the chemical diffusion coefficient from hydrogen permeation experiments. Corrosion Sci 2014;82:93–100.
[80] Van den Eeckhout E, Laureys A, Van Ingelgem Y, Verbeken K. Hydrogen permeation through deformed and heat-treated Armco pure iron. Mater Sci Technol 2017;33(13):1515–23.
[81] Drexler A, Siegl W, Ecker W, Tkadletz M, Klösch G, Schnideritsch H, Mori G, Svoboda J, Fischer FD. Cycled hydrogen permeation through Armco iron – a joint experimental and modeling approach. Corrosion Sci 2020;176(June).

[82] Zafra A, Peral LB, Belzunce J. Hydrogen diffusion and trapping in A 42CrMo4 quenched and tempered steel: influence of tempering temperature. Int J Hydrogen Energy 2020;45(55):31225–42.
[83] ASTM G148-97(2018). Standard practice for evaluation of hydrogen uptake, permeation, and transport in metals by an electrochemical technique. 2018.
[84] Fallahmohammadi E, Bolzoni F, Lazzari L. Measurement of lattice and apparent diffusion coefficient of hydrogen in X65 and F22 pipeline steels. Int J Hydrogen Energy 2013;38(5):2531–43.
[85] Turnbull A. Hydrogen transport and cracking in metals. Teddington, UK: Institute of Materials, National Physical Laboratory; 1994.
[86] Zhang TY, Zheng YP. Effects of absorption and desorption on hydrogen permeation - I. Theoretical modeling and room temperature verification. Acta Mater 1998;46(14):5023–33.
[87] Zakroczymski T. Electrochemical method for hydrogen determination in steel. Corrosion 1982;38(4):218–23.
[88] Caskey GR, Pillinger WL. Effect of trapping on hydrogen permeation. Metall Trans A 1975;6(3):467–76.
[89] López-Suárez A. Influence of surface roughness on consecutively hydrogen absorption cycles in Ti-6Al-4V alloy. Int J Hydrogen Energy 2010;35(19):10404–11.
[90] Makhlouf MM, Sisson RD. Modeling surface effects on hydrogen permeation in metals. Metall Trans A 1991;22(5):1001–6.
[91] Zhang T, Zheng Y, Wu Q. On the boundary conditions of electrochemical hydrogen permeation through iron. J Electrochem Soc 1999;146(5):1741–50.
[92] Zakroczymski T, Szklarska-Smialowska Z, Smiakowski M. Effect of promoters on the permeation of electrolytic hydrogen through steel. Werkstoffe Korrosion 1976;27:625–30.
[93] Juang CC, Wu JK. The effect of chemical additives on the kinetics of the absorption of hydrogen in steel. Corrosion Sci 1994;36(10):1727–33.
[94] Pumphrey P. On the boundary conditions for hydrogen permeation through cathodically charged iron and mild steel. Scripta Metall 1980;14(c):695–701.
[95] Sun YW, Chen JZ, Liu J. Investigation into hydrogen diffusion and susceptibility of hydrogen embrittlement of high strength 0Cr16Ni5Mo steel. J Iron Steel Res Int 2015;22(10):961–8.
[96] Wang JS. On the diffusion of gases through metals. Math Proc Camb Phil Soc 1936;32(4):657–62.
[97] Bockris JO, McBreen J, Nanis L. The hydrogen evolution kinetics and hydrogen entry into a-iron. J Electrochem Soc 1965;112(10):1025–31.
[98] Akiyama E, Li S. Electrochemical hydrogen permeation tests under galvanostatic hydrogen charging conditions conventionally used for hydrogen embrittlement study. Corrosion Rev 2015;34(1–2):103–12.
[99] Liu Q, Venezuela J, Zhang M, Zhou Q, Atrens A. Hydrogen trapping in some advanced high strength steels. Corrosion Sci 2016;111:770–85.